Journal of Marine Science and Technology

Volume 28 | Issue 4 Article 6

DESIGN OF AN OPTIMAL ADAPTIVE INTELLIGENT CONTROL SCHEME FOR STATCOM IN A SERIES COMPENSATED WIND FARM

Fei Wang
School of Information Technology, Beijing Institute of Technology, Zhuhai, China

Kai-Hung Lu
School of Information Technology, Beijing Institute of Technology, Zhuhai, China School of Electronic and Electrical Engineering, Minnan University of Science and Technology, Fujian, China, khluphd@163.com

Qiangqiang Xu
School of Information Technology, Beijing Institute of Technology, Zhuhai, China

Ziwen Chen
School of Information Technology, Beijing Institute of Technology, Zhuhai, China

Journal of Marine Science and Technology, Vol. 28, No. 4, pp. 276-287 (2020)
DOI: 10.6119/JMST.202008_28(4).0006

DESIGN OF AN OPTIMAL ADAPTIVE INTELLIGENT CONTROL SCHEME FOR STATCOM IN A SERIES COMPENSATED WIND FARM

FeiWang[1], Kai-Hung Lu[*,1,2], Qiangqiang Xu[1] and Ziwen Chen[1]

Key words: Static synchronous compensator, Functional-link based Elman neural network, Genetic algorithm hybrid time varying particle swarm optimization, Optimal adaptive intelligent controller.

ABSTRACT

This paper proposes a static synchronous compensator (STATCOM) for use with a self-excited induction generator (SEIG)-based wind farm. The STATCOM applies a damping controller based on an optimal adaptive intelligent controller (OAIC) comprising the critical network, the functional link-based Elman neural network (FLENN), and the genetic algorithm hybrid time-varying particle swarm optimization (GAHTVPSO) algorithm. The OAIC improves the damping power oscillations in the SEIG-based series-compensated wind farm system. The node-connecting weights of the proposed FLENN and the critical network are trained online via a backpropagation (BP) algorithm, and the GAHTVPSO adjusts the learning rates of the BP algorithm to improve the learning ability of the neural network. A performance analysis confirms the superior damping characteristics of the proposed controller. Moreover, the internal power fluctuations to the power system can be effectively alleviated under variable wind-power generation conditions.

I. INTRODUCTION

Wind generation systems are receiving considerable attention as they are safe, renewable, and clean power sources. Various control strategies that achieve the desired speed control of wind generators have been proposed (Waldner and Erlich, 2014). In all types of wind induction generators, the most important characteristic is the self-excitation effect. The so-called self-excited induction generator (SEIG) offers the best control performance in an isolated system. The rated voltage is set by the SEIG excitation capacitor connected to the stator terminal. Sub-synchronous resonance (SSR) is an important state of a power system, in which the power network exchanges energy with the SEIG-based wind turbine generator at the fundamental frequencies of the combined power system below the sub-synchronous frequency (Golshannavaz et al., 2011). SSR occurs via energy interchange between the series capacitors on the transmission lines and the mass–spring system of the turbine-generator shaft. The SSR phenomenon can lead to failure of the wind turbine generator shaft and instability of the wind farm at the end of the series-compensated transmission lines.

The static synchronous compensator (STATCOM) proposed by Gyugyi and Hingorani is the most versatile and powerful flexible alternating-current transmission system (Singh et al., 2014, Elsamahy et al., 2014a, Elsamahy et al., 2014b). The STATCOM increases the system security by increasing the transient stability limit, limiting the short circuit currents and overloads, and alleviating blackouts and damping oscillations of power systems. Therefore, for mitigating SSR, STATCOM is the most suitable device. Recently, several studies have proposed STATCOM control methods that improve the damping of low-frequency power oscillations in power systems (Mohamed El-Moursi et al., 2010). In one approach, the physical control loops have been embedded in state feedback control techniques that mitigate the oscillations (Chen et al., 2010), whereas the other approach (Fan and Miao, 2012) includes the design of auxiliary SSR damping controller and selection of control signals. However, the former approach makes only a limited improvement, while the latter approach is of limited applicability because the design of the controller is very complicated to be suitable for large-scale wind farms. STATCOM-based methods have their own limitations because the wind-farm power systems to which the STATCOM is connected are themselves very complex. This complexity reduces the efficiency

Paper submitted 09/03/18; revised 08/26/19; accepted 05/12/20. Corresponding Author: Kai-Hung Lu (Email: khluphd@163.com)
[1] School of Information Technology, Beijing Institute of Technology, Zhuhai, China
[2] School of Electronic and Electrical Engineering, Minnan University of Science and Technology, Fujian, China

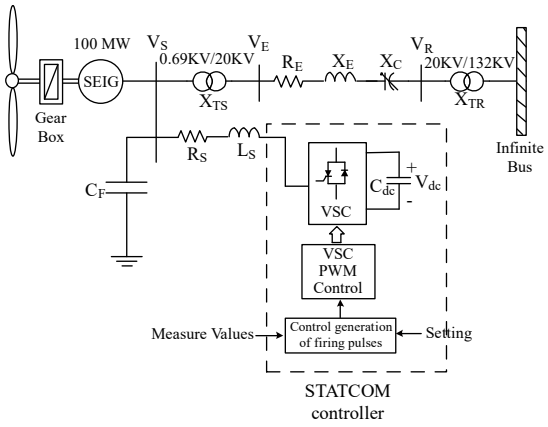

Fig.1. Configuration of the STATCOM system with a series- compensated power system of a SEIG wind farm

of the control schemes in mitigating SSR, thus degrading the control performance. Other studies have proposed external controllers using intelligent control schemes such as fuzzy logic controllers, neuro-fuzzy external controllers, hybrid fuzzy/linear quadratic regulator controllers, and a gray-based genetic algorithm (Salman et al., 2007; Hong and Luo, 2009; Li and Dinh-Nhon, 2013). Although these intelligent controllers have improved the control of low-power oscillations by STATCOM, many parameters in these algorithms (such as the learning rate) must be determined by trial-and-error. To remove the above problems, this paper proposes an optimal adaptive intelligent controller (OAIC) for STATCOM that mitigates SSR and dampens the power-system oscillations. The proposed OAIC considerably improves the limitations of the previous studies, and is more suitable for complex, unstable, and stochastic wind farms compared to the existing methods. The OAIC comprises the critical network, a functional link-based Elman neural network (FLENN), and the genetic algorithm hybrid time-varying particle swarm optimization (GAHTVPSO) algorithm.

The Elman neural network (ENN) is a partially recurrent network model proposed by Elman in 1990 (Lin et al., 2013). An Elman network is dynamically characterized by its internal connections, and does not require the system state as an input or training signal. Because it out performs static feed-forward networks, the ENN is extensively applied in dynamic systems, but its convergence and training speed are usually very slow, precluding the algorithm's use in complex systems. Instead, this study adopts the FLNN, which improves the performance of ENN by inputting linearly independent trigonometric basis functions, which are used for functional expansion of the FLNN in the extended classification space. Moreover, the FLNN can capture the nonlinear input–output relationships among a suitable set of polynomial inputs because the high-order effects are incorporated in the higher dimensions of the input-variable space. In this manner, the FLNN can effectively approximate a nonlinear function (Lin et al., 2009; George and Panda, 2012); therefore, it is suitable for complex power system applications such as the wind-farm system examined in this study.

Particle swarm optimization (PSO), pioneered by Kennedy and Eberhart in 1995 (Toh and Yau, 2005; Chen et al., 2007; George and Panda, 2012), was inspired by social animal behaviors such as fish schooling, bird flocking, and swarming. The genetic algorithm is another population-based and self-adaptive optimization tool, which has optimally solved difficult multidimensional discontinuous problems in various fields (Lin et al., 2009). Unlike GA, PSO can retain the knowledge of good solutions, which is known to all particles. A recently proposed parameter-tuning approach, called PSO time-varying acceleration coefficients, has been shown to improve the performance of PSO (Srivastava et al., 2012; 2014). The present study proposes an OAIC for STATCOM that mitigates SSR and dampens the power-system oscillations. The OAIC is intended to improve the intransient stability of the STATCOM damping controller. The transient system responses of the system to three-phase short circuit faults and changing wind conditions are investigated in an integrated (SEIG)-based wind farm. Without retuning, conventional controllers deliver poor performance under such changes; however, this weakness is overcome by the FLENN approach. The critical network estimation is related to the FLENN controller, ensuring the optimal damping control signal to the STATCOM. However, the initial values of FLENN and the critical network learning rates are normally difficult to obtain. Therefore, this study also optimizes the learning rates byapplying a crossover operation to the particles' chromosomes in the GAHTVPSO algorithm.

II. ANALYSIS OF SYSTEM MODELS

Fig. 1 shows the system examined in this study (Mohamed El-Moursi et al., 2010). The system contains100 MW SEIG-based wind turbine generators connected to the electric grid through a fixed series-compensated SATCOM-based transmission system and a transformer X_{TS}. The compensation capacitor X_c improves the power factor of the power grid; reduces the loss of the power supply transformer and transmission line; and improves the power supply efficiency and the quality of the power grid. The proposed STATCOM has a rated capacity of 70MVar, and its voltage source converter (VSC) is connected in shunt with the AC power system via a shunt transformer T_{sh}, which primarily satisfies the real power demand at the common DC link. The SEIG provides the required reactive power via the shunt capacitor C_F. Because the capacitor demand for excitation varies with the speed of the induction generator (IG), C_F is connected across Bus S of the IG, whose voltage V_s varies with generator speed. The parameters of the studied system are listed in the Appendix.

2.1 Wind Turbine Characteristics

The wind turbine intakes the variable wind and outputs the mechanical power that turns the generator rotor blades (Lin

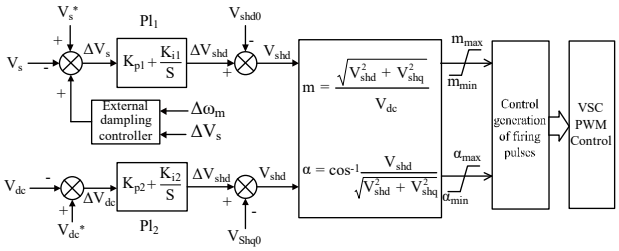

Fig. 2 Internal controller of STATCOM

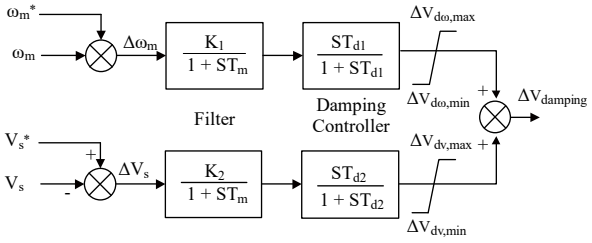

Fig. 3 Externallinear damping controller of STATCOM

et al., 2011; Lin et al., 2013). The available mechanical power output by a wind turbine is obtained as follows:

$$P_m \frac{1}{2}\rho A C_p(\lambda,\beta)V_\omega^3 \tag{1}$$

Equation (1) is anonlinear function of the tip speed ratio (TSR) λ where

$$\lambda = \frac{\omega_r \bullet r}{V_\omega} \tag{2}$$

Note that C_p is a function of the TSR and β, and isgenerally defined as follows (Lin et al., 2011; Lin et al., 2013):

$$C_p = 0.517\left(\frac{116}{\lambda_i} - 0.4\beta - 5\right)e^{\frac{-21}{\lambda_i}} + 0.0068\lambda \tag{3}$$

Giving

$$\lambda_i = \frac{1}{\frac{1}{\lambda - 0.08\beta} - \frac{0.035}{\beta^3 + 1}} \tag{4}$$

2.2 SEIG

The wind generator chosen for this study is a three-phase SEIG, where T_m and T_e are expressed as follows (Eberhart and Shi, 2014; Farkhani and Najafi, 2014):

$$T_m = \frac{P_m}{\omega_r} \tag{5}$$

$$T_e = \frac{P_e}{\omega_e} = \frac{2}{n_p}\frac{P_e}{\omega_r} \tag{6}$$

In general, the torque equation of a SEIG is obtained using the following:

$$J\frac{d\omega_r}{dt} = T_m - B\omega_r - T_e \tag{7}$$

The machine model of a SEIG can be described in the rotor-rotating reference frame as follows:

$$\begin{aligned} v_q &= Ri_q + p\lambda_q + \omega_s\lambda_d \\ v_d &= Ri_d + p\lambda_d + \omega_s\lambda_q \end{aligned} \tag{8}$$

With

$$\begin{aligned} \lambda_q &= L_q i_q \\ \lambda_d &= L_d i_d + L_{md} I_{fd} \end{aligned} \tag{9}$$

$$\omega_s = n_p\omega_r \tag{10}$$

2.3 STATCOM external control

The STATCOM of the shunt device be haves as a synchronous compensator but without inertia. The STATCOM provides both capacitive and inductive compensation, supporting the bus voltage by independently controlling its output current. The real current controls the real power, while the active current controls the reactive power and exchanges it between the STATCOM and the power system. Moreover, the STATCOM improves the stability of the power system. The STATCOM is controlled by external auxiliary control loops that dampen the SSR, thus improving the reference signal of the line voltage controller. The basic control structure of the STATCOM is shown in Fig. 2.

In this figure, V_S^* and V_{dc}^* are the reference signals of the bus voltage and the dc link voltage of STATCOM, respectively. Furthermore, K_{p1}, K_{p2}, K_{i1}, and K_{i2} are the proportional and integral gains of their corresponding PI controllers. V_{shq0} and V_{shd0} are the initial voltages along the quadrature (q) and direct (d) axes, respectively, in the synchronous reference frame. The m and α derived from the direct and quadrature voltage components are then provided to the PWM generator that provides the gating signals for the power electronic switches in the VSC.

The external damping controller of STATCOM (composed of the filter and damping controller; Fig. 3) improves the dynamic stability of the system. The inputs of the damping loops are the generator speed deviation $\Delta\omega_m$ (which is easily obtained by measurement and analysis) and the terminal voltage deviation ΔV_S relative to the external controller. The primary function of STATCOM is regulating the line voltage at the connection point, and hence damping all SSR modes in all series compensations. However, under the varying operating conditions of the power system, the performance of the linear

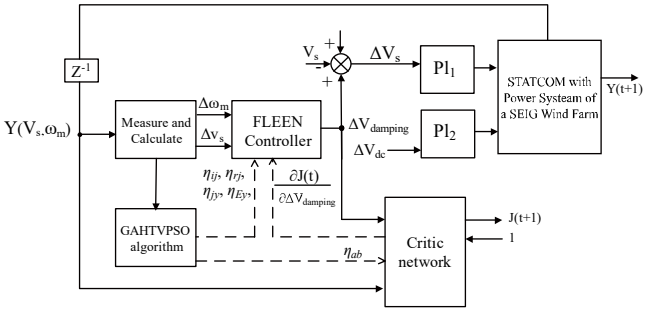

Fig. 4 OAIC for STATCOM

external controller will be significantly affected by changes in wind speed. To optimize the performance of the power system, the controller parameters are fine-tuned at a single operating point

III. OAIC DESIGN FOR THE DAMPING CONTROLLER

The input signal of the damping controller should be in phase with the generator rotor speed deviation $\Delta\omega_m$ and the variation of terminal voltage ΔV_S. The proposed OAIC comprises three parts: the adaptive critic network, the FLENN, and the GAHTVPSO algorithm, as shown in Fig. 4. The function expansion in the FLENN improves the accuracy of the function approximation. The proposed FLENN and critic network is configured using the online tuning learning rates by the GAHTVPSO. The adaptive critic network (Swakshar and Ganesh, 2008; 2013) provides suitable training signals for the FLENN controller. The proposed OAIC can provide near-optimal results in complex and uncertain nonlinear systems; hence, it can solve the Hamilton–Jacobi–Bellman equation of optimal control (Swakshar and Ganesh, 2008; 2013).

3.1 FLENN

Fig. 5 shows the design of the FLENN controller. The network comprises an input layer, a hidden layer governed by a sigmoidal function $S(x)=1/(1+e^{-x})$, a context layer, and an output layer connected to an FLNN. The context layer is fed back to itself with a time delay z^{-1}. Using a feed forward neural network structure, the FLNN generates a set of linearly independent functions, and then functionally expands the elements of the input variables. The trigonometric functions in the FLNN are more quickly computed than Gaussian, sine, and cosine functions. Moreover, the FLNN improves the performance results when the outer product term is included in the function expansion (George and Panda, 2012). The input vector $\boldsymbol{X}=[X_1, X_2]^T$, a functional expansion of a trigonometric polynomial basis function, can be written in the enhanced space as $\boldsymbol{\psi}=[\psi_1, \psi_2,\ldots\psi_p]=[1, X_1, \sin(\pi X_1), \cos(\pi X_1), x_2, \sin(\pi X_2), \cos(\pi X_2), X_1X_2]$, where $X_1X_2$is the outer product term. Furthermore, the FLNN output is expressed as the linear sum of the yth node, as follows:

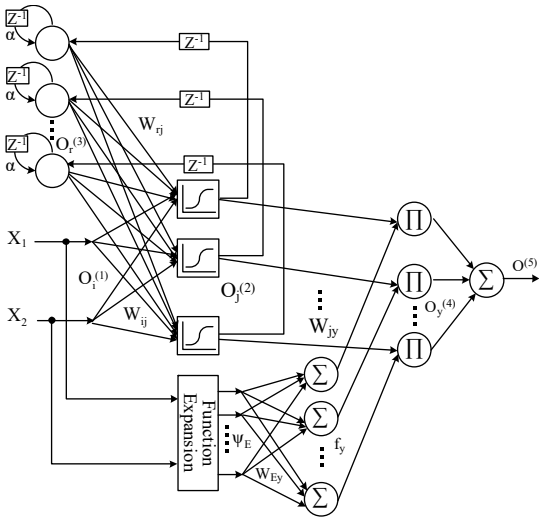

Fig. 5 Design of the FLENN controller

$$\hat{f}_y(k)=\theta\left(\sum_E \psi_E(x_i)\cdot w_{Ey}\right)=\theta\left(w_{Ey}\cdot\psi_E(\boldsymbol{X})\right) \tag{11}$$

Using the FLENN input $\boldsymbol{X}=[\Delta\omega_m, \Delta V_S]^T$, the power system directly transmits the numerical inputs to the next layer. The context neurons of the FLENN serve as memory units that store the output signal of the hidden layer. The FLENN can exploit these context neurons to increase the dynamic characteristics of the network. The node outputs O of each FLENN layer are superscripted by their layer number and subscripted by the signal number of their related output as follows:

$$O_i^{(1)}(t)=X_i^{(1)}(t), i=1,2 \tag{12}$$

$$O_j^{(2)}(t)=\sum_i O_i^{(1)}(t)\cdot w_{ij}+\sum_i O_r^{(3)}\cdot w_{rj} \tag{13}$$

$$O_r^{(3)}(t)=\alpha O_r^{(3)}(t-1)+O_j^{(2)}(t-1) \tag{14}$$

$$O_m^{(4)}(t)=\hat{f}_y\prod_{y=1}^{9} O_j^{(2)}(k)\cdot w_{jy} \tag{15}$$

$$O^{(5)}(t)=\sum_y O_y^{(4)}(k)\cdot w_o \tag{16}$$

The objective of the FLENN controller is to train the parameters w_{ij}, w_{rj}, w_{jy}, and w_{Ey}t o determine the best match to the control signal $O^{(5)}=\Delta V_{damping}$. This output is added to the voltage reference V_s* of the PI_1 controller (Fig. 4).

3.2 Critic network

A critic network can be continuously trained to learn the cost-to-go function associated with the power system. This

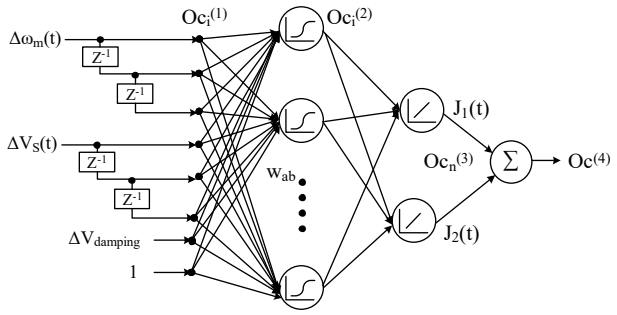

Fig.6 Critic network

ability is paramount in real time optimal-control operations subjected to changes in configuration and operating conditions. The cost-to-go function J in Bellman's equation of dynamic programing is then estimated by the critic network as follows (Swakshar, 2013):

$$\begin{aligned} J(t) &= \sum_{k=0}^{\infty} \gamma^k U(t+k) \\ &= U(t) + \sum_{k=0}^{\infty} \gamma^k U\left[(t+1)+k\right] \\ &= U(t) + \gamma \cdot J(t+1) \end{aligned} \tag{17}$$

Here, the utility function $U(t)$determines the form of the optimal cost-to-go function, and γ represents the discount factor (0–1). The utility functions $U_a(t)$ and $U_b(t)$ of the critic network are determined by

$$U_a(t) = \left|\Delta\omega_m(t) + \Delta\omega_m(t-1) + \Delta\omega_m(t-2)\right| \tag{18}$$

$$U_b(t) = \left|\Delta V_S(t) + \Delta V_S(t-1) + \Delta V_S(t-2)\right| \tag{19}$$

The total utility function is then obtained as follows:

$$U(t) = U_a(t) + U_b(t) \tag{20}$$

The node output O_c of each layer of the critic network is superscripted by its layer number and subscripted by the signal number of its related output as follows:

$$Oc_i^{(1)}(t) = X_i^{(1)}(t),\ \boldsymbol{X} = [\Delta\omega_m(t), \ldots \Delta V_S(t-1), \ldots 1] \tag{21}$$

$$Oc_i^{(2)}(t) = \frac{1}{1+exp^H}, H = \sum_{i=1}^{8} Oc_i^{(1)} w_{ab} \tag{22}$$

$$Oc_n^{(3)}(t) = J_n(t) = \sum_{n=1}^{2} Oc_i^{(2)} \tag{23}$$

$$Oc^{(4)}(t) = \sum Oc_n^{(3)} = J(t) \tag{24}$$

Eqs. (18) and (19) are expected to improve the STATCOM performance of both the generator speed deviation $\Delta\omega_m$ and the line voltage deviation ΔV_S. The critic network in Fig. 6 has a four-layer feed-forward network structure. After the training process, the critic network optimally controls the minimization of $J(t)$. Accordingly, the FLENN controller optimizes the damping control signal provided to the STATCOM.

3.3 Training process of the FLENN and critic network

The gradient of the error function defines the direction of change of the function. Therefore, searching the opposite side of the gradientwill minimize the cost-to-go function. In the present study, the error function E in the gradient descent algorithm was assumed as themean squared error function (Swakshar and Ganesh, 2008).

$$\begin{aligned} E &= \frac{1}{2}\left[J^*(t) - J(t)\right]^2 \\ &= \frac{1}{2}\left[U(t) + \gamma \cdot J^*(t+1) - J(t)\right]^2 \end{aligned} \tag{25}$$

where $J^*(t)$ is the reference value of the cost-to-go function.

When handling deviation signals, $J^*(t)$ is set to zero.

The changes in a BP algorithm are directly proportional to the amount by which the weights w_{ab} are modified. Therefore, they can estimate the instantaneous changes in the negative gradient. In the online algorithm of the critic network and proposed FLENN, the gradient is computed by the chain rule as shown in Eqs. (26) and (27). The weights w_{ab} of the critic network and the weights W_{FLENN} of the FLENN are adjusted by Eqs. (27) and (28), respectively. The training procedure is detailed in a previous study (Lin et al., 2011).

$$\frac{\partial E}{\partial w_{ab}} = \frac{\partial E}{\partial J} \cdot \frac{\partial J}{\partial w_{ab}} \tag{26}$$

$$\frac{\partial E}{\partial W_{FLENN}} = \frac{\partial E}{\partial J} \cdot \frac{\partial J}{\partial O^{(5)}} \cdot \frac{\partial O^{(5)}}{\partial W_{FLENN}} \tag{27}$$

$$w_{ab}(t+1) = w_{ab}(t) - \eta_{ab} \cdot \frac{\partial E(t)}{w_{ab}(t)} \tag{28}$$

$$W_{FLENN}(t+1) = W_{FLENN}(t) - \eta_{FL} \cdot \frac{\partial E(t)}{W_{FLENN}(t)} \tag{29}$$

where η_{ab} is the learning rate of w_{ab}, $W_{FLENN} = [w_{ij}, w_{rj}, w_{jy}, w_{Ey}]$, and $\eta_{FL} = [\eta_{ij}, \eta_{rj}, \eta_{jy}, \eta_{Ey}]$ are the learning rates of W_{FLENN}.

The learning rate values η_{ij}, η_{rj}, η_{jy}, η_{Ey}, and η_{ab} of the OAIC should be properly set in the BP algorithm. If the learning rate

is too large or too small, the progress of the BP algorithm is compromised and the learning process may fail. To avoid this possibility, the optimal learning parameters in the present study are optimized by the GAHTVPSO algorithm.

3.4 Adjustment of Learning Rates by the GAHTVPSO Algorithm

To further improve the online learning ability of the OAIC, the learning rates η_{ij}, η_{rj}, η_{jy}, η_{Ey}, and η_{ab} are tuned by the GAHTVPSO algorithm, in which each particle adjusts its position according to its own experience and those of its neighbors. The "experience" parameters include the current velocity, current position, and the best previous position of a particle and its neighbors.

Stochasticity in the algorithm is introduced by two pseudo-random sequences r_1~U(0, 1) and r_2~U(0, 1). Let R_i^d and $pbest_i^d$ be the current position and current personal best position respectively, where d is the dimension of the search space. The velocity update law is given by Eq. (30), and the inertia weight is set to ω=0. The parameter settings are reduced by the GAHTVPSO algorithm. Eqs. (31) and (32) modify the time-varying acceleration coefficients c_1 and c_2, respectively (Srivastava et al., 2014).

$$v_i^d(N+1) = \omega v_i^d(N) + c_1 \bullet r_1 \bullet \left(pbest_i^d - R_i^d(N)\right) + c_1 \bullet r_2 \bullet \left(gbest_i^d - R_i^d(N)\right) \tag{30}$$

$$c_1 = \left(c_{1f} - c_{1i}\right) \cdot \frac{N}{N_{max}} + c_{1i} \tag{31}$$

$$c_2 = \left(c_{2f} - c_{2i}\right) \cdot \frac{N}{N_{max}} + c_{2i} \tag{32}$$

$$R_i^d(N+1) = R_i^d(N) + v_i^d(N+1) \tag{33}$$

Where v_i^d and R_i^d are the current velocity and position of the particle, respectively. N_{max} is the maximum number of iterations. c_{1i} and c_{2i} are the initial parameter settings, and c_{1f} and c_{2f} are the final parameter settings.

Step 1: Define the basic conditions

The current positions R_i^d= [R_1, R_2, R_3, R_4, R_5] and learning rates (η_{ij}, η_{rj}, η_{jy}, η_{Ey} and η_{ab}) must be optimized within their minimum and maximum ranges.

Step 2: Initialize the location and velocity

The initial locations $R_i^d(N)$ and velocities $v_i^d(N)$ of all particles are randomly generated in the search space. The initial *p*best of a particle is initialized by its current position and the *g*best of a group is selected from among the *p*bests. The elements in the vector $R_i^d(N)$ are randomly generated by the following equation:

$$R_i^d\, U\left[\eta_{min}^d, \eta_{max}^d\right] \tag{34}$$

where $U[\eta_{min}^d, \eta_{max}^d]$ designates the outcome of auniformly distributed random variable ranging overthe given lower and upper bounded values η_{min} and η_{max} of a learning rate.

Step 3: Determination of the fitness function

Each vector R_i^d, must be assigned with a fitness value. In this study, the fitness values were calculated by the following fitness function:

$$FIT = \frac{1}{0.1 + abs\left(\omega_m - \omega_m^*\right) + abs\left(V_s - V_S^*\right)} \tag{35}$$

where *FIT* is the fitness value and $abs(\cdot)$ is the absolute function. The small constant 0.1 prevents the denominator from approaching infinity.

Step 4: Selection of pbest and gbest:

Each particle R_i^d memorizesits own fitness value and selects its personal best from its own track record as $pbest_i^d$. The maximum vector in the population of $pbest_i^d$ vector $\left[pbest_1^d, pbest_2^d, \cdots pbest_p^d\right]$is then obtained. Moreover, each particle R_i^d is preset to $pbest_i^d$in the firstiteration, and the particle with the best fitness value among the various pbests is assumed as the global gbest.

Step 5: Check for updates in gbest:

The gbest particle position does not change over some designated time steps, but is eventually changed by a crossover operation on its GA chromosome. The position and velocity are reorganized as follows:

$$R_i^d(N+1) = c_3 \cdot rand(\bullet) \cdot \left(gbest_i^d - R_i^d(N)\right) \tag{36}$$

$$\begin{cases} p_{child1} = \beta p_{parent1} + (1-\beta) p_{parent2} \\ p_{child2} = \beta p_{parent2} + (1-\beta) p_{parent1} \end{cases} \tag{37}$$

$$\begin{cases} v_{child1} = \dfrac{v_{parent1} + v_{parent2}}{\left|v_{parent1} + v_{parent2}\right|} \cdot \left|v_{parent1}\right| \\ v_{child2} = \dfrac{v_{parent1} + v_{parent2}}{\left|v_{parent1} + v_{parent2}\right|} \cdot \left|v_{parent2}\right| \end{cases} \tag{38}$$

where c_3 is the acceleration factor, and rand() represents a uniform random number between 0 and 1. p_{parent} and p_{child} are the parent and child generations of the current position, respectively. Similarly, v_{parent} and v_{child} are the parent and child generations of the velocity, respectively. β is the interpolation value between the parent and child generations, and is selected from a uniform random distribution between 0 and 1.

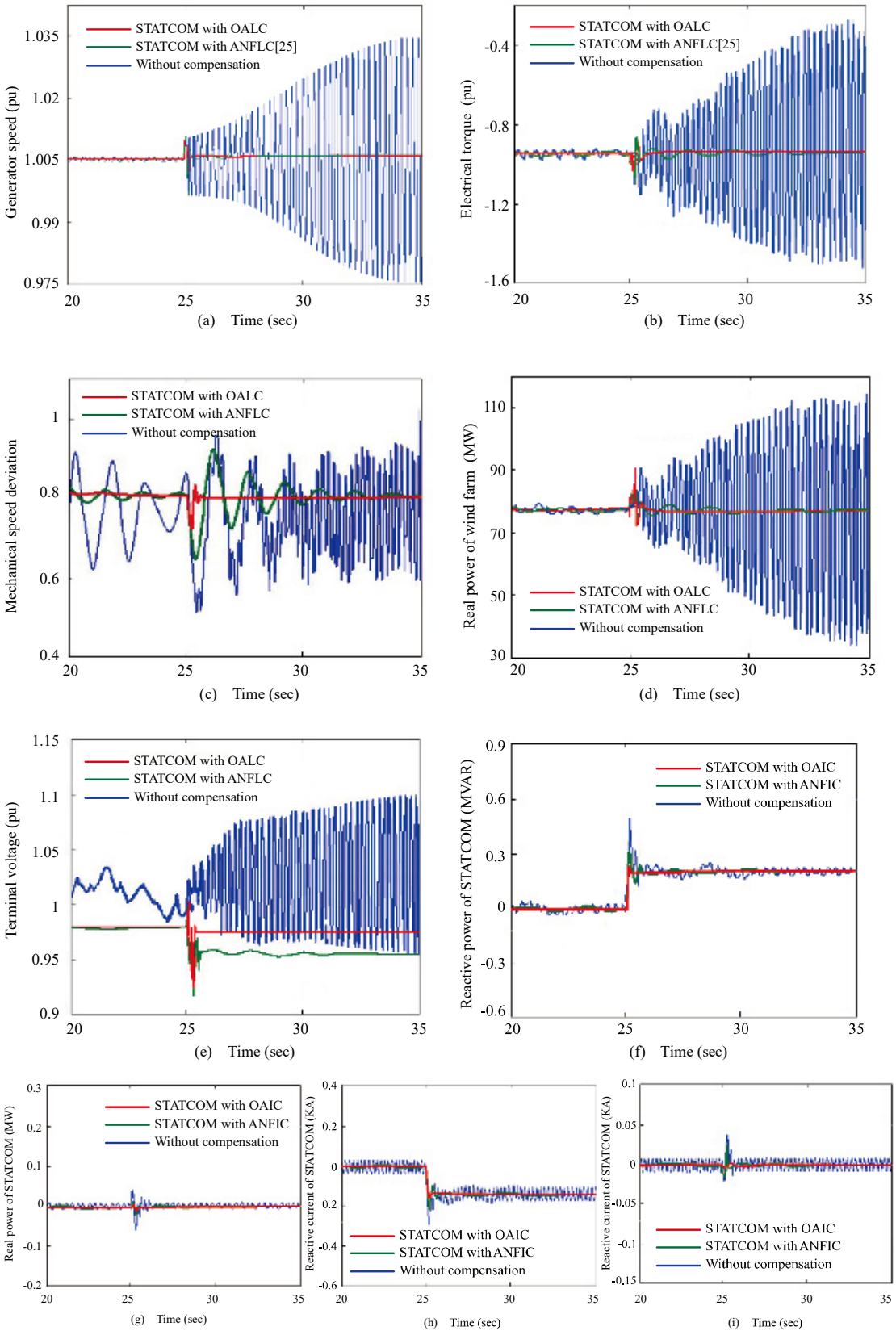

Fig. 7 Comparison results of Case 1. Plotted are the (a)generator speeds, (b) electrical torque responses, (c) mechanical speed deviations, (d)real power of the wind farm, (e) voltage of the bus terminal, (f) reactive power in STATCOM, (g) real power in STATCOM, (h) reactive current in STATCOM, and (i) real current in STATCOM.

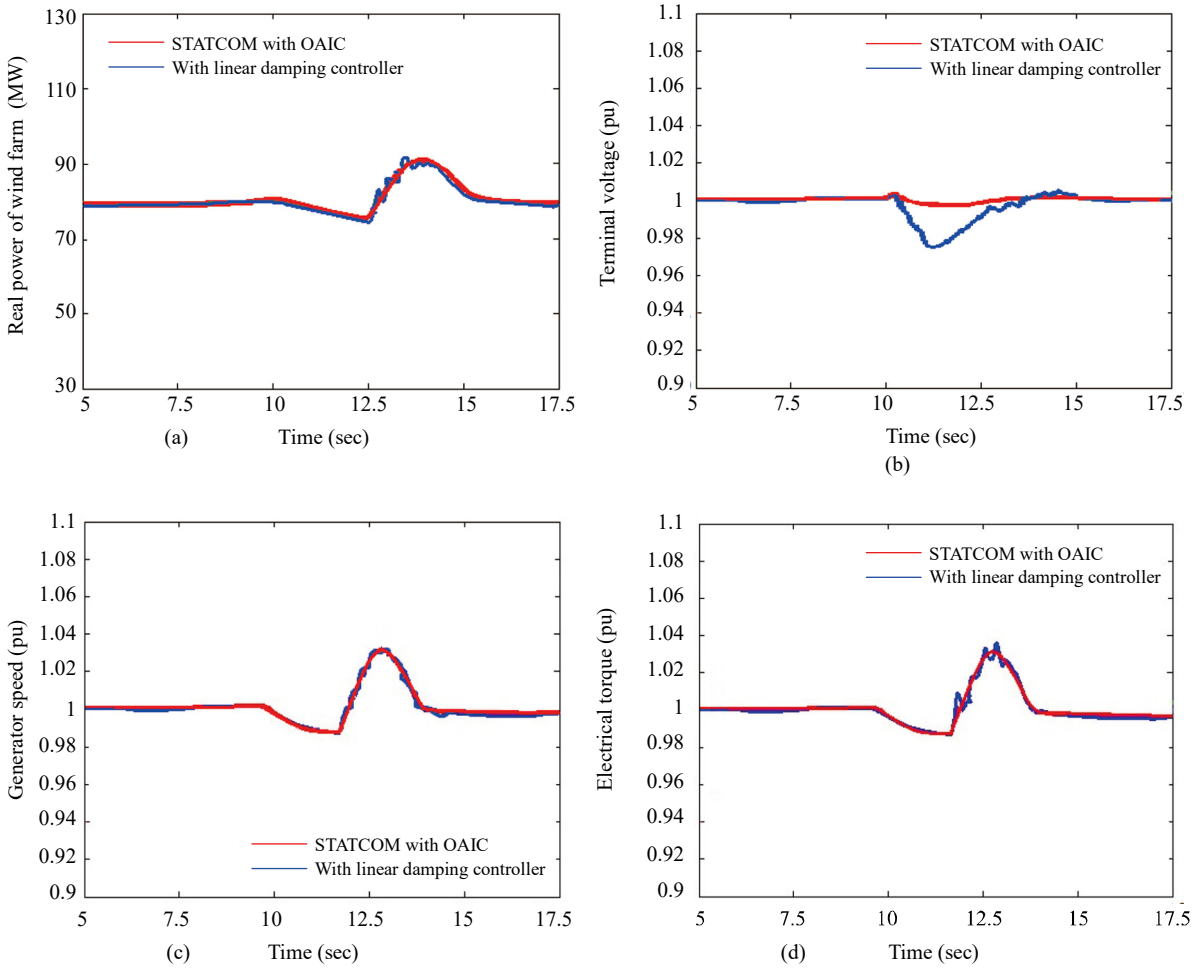

Fig. 8 Comparison results of Case 2. Plotted are (a) real power of the wind farm, (b) voltage of the bus terminal, (c) generator speed, and (d) electrical torque responses.

Step 6: Update the velocity and position

Adding the new velocity to the current position of the particle, the next position of the particle is calculated by Eqs. (30) and (33).

Step 7: Check for convergence

Steps 3–6 are repeated until the best fitness value of gbest is not obviously improved, or until a specified number of generations are reached. The final highest-fitness value $gbest_i^d$ is the optimal learning rate (η_{ij}, η_{rj}, η_{jy}, η_{Ey} and η_{ab})of the OAIC.

IV. CASE STUDY

The damping enhancement of a wind farm system installed with the OAIC was evaluated in a simulation case study. The series-compensated wind farm in Fig. 1 (Mohamed El-Moursi et al., 2010) was built in a PSCAD/EMTDC environment. The FLENN and critic network controllers with the GAHTVPSO algorithm were implemented in a MATLAB program module. The parameters and initial values of the system were similar to those in an earlier work (Mohamed El-Moursi et al., 2010), and are given in the Appendix. The following cases illustrate the proposed method under different operating conditions.

4.1 Case1: Series-capacitive compensation

The series-compensated wind farm was simulated while increasing the series-capacitive compensation from 0.15 to 0.3pu at 25-second intervals. To examine whether the proposed OAIC outperforms other intelligent control systems, the OAIC results were compared with those of the adaptive neuro fuzzy inference controller (ANFIC) algorithm (Farrag and Putrus, 2012) using the parameters of the earlier work (Farrag and Putrus, 2012). Fig. 7 (a) compares the generator speeds without compensation, with STATCOM plus ANFIC (Farrag and Putrus, 2012), and with STATCOM plus the proposed OAIC. When STATCOM is installed with the proposed OAIC damping controller, the variations in generator speed were significantly reduced. Panels (b) and (c) of Fig. 7 compare the electrical torque responses and the mechanical speed deviations in each system, respectively. The uncompensated system was subjected to SSR resonance caused by torsional modes, and the mechanical speed was easily diverged. STATCOM

Table 1.Performance results ofseveral methods

Method	Interactive Number	CPU Time(s)	Mean Square Error (10^{-3})	Accuracy (%)
GAHTVPSO	37	1.48	1.23	98.77
MPSO	33	1.32	4.36	95.64
IPSO	57	2.28	5.08	94.92
Fuzzy	98	3.92	12.35	87.65

Table 2. Normalized performance indices in all cases

PI of normalized Case	Without STATCOM	Linear damping controller	ANFIC [25]	OAIC
Case 1	1.0	1.39	1.62	1.86
Case 2	1.0	1.58	2.13	2.41
Case 3	1.0	1.73	1.93	2.31
Overall	1.0	1.56	1.72	2.19

installed with the OAIC damping controller clearly improved the power-system performance by mitigating the SSR.

The wind farm maintained the real power at 80 MW with respect to the transmission line (Fig. 7(d)). In the bus terminal voltage control (Fig. 7(e)), the STATCOM generated a small reactive power of 0.15 MVar (Fig. 7(f)) to maintain the bus voltage. It also changed the reactive power while maintaining the real power at the desired level (Fig. 7(g)). Fig. 7(h) and (i) show the reactive and real currents in STATCOM, respectively. The real current controls the real power, while the reactive current controls the reactive power exchanged between STATCOM and the power system. In this case, the proposed OAIC damping controller for STATCOM exerted a stronger damping effect than the proposed ANFIC (Farrag and Putrus, 2012).

4.2 Case2: Stability against wind speed change

The wind speed was changed from 14 to 11 m/s at the 10th second, and from 10 m/s to 14 m/s at the 15th second. Fig. 8(a) compares the real-power responses to these changes in the transmission line under linear damping control and STATCOM with OAIC control. The wind-speed variations affected the real power of the SEIG-based wind farm. When the STATCOM with OAIC was installed, the amplitudes of the real power changes were reduced, implying improved control. Similarly, changing the wind speed altered the voltage magnitudes of the bus (Fig. 8(b)). Obviously, combining the designed OAIC damping controller with the STATCOM suppressed the voltage variations and regulated the terminal bus voltage to 1 pu. The dynamic damping of the electrical torque and the rotor speed oscillations in the wind turbine are shown in Figs. 8(c) and (d), respectively. The proposed OAIC achieved better control than the linear damping controller, and clearly suppressed the variations. However, both damping controls effectively mitigated the power oscillation and improved the system stability.

Fig. 8 Comparison results of Case 2. Plotted are (a) real power of the wind farm, (b) voltage of the bus terminal, (c) generator speed, and (d) electrical torque responses.

4.3 Case3: Transient stability against a three- phase fault

A three-phase short circuit (of duration 0.1 s) was simulated at the 25th second. In this scenario, the damping characteristics of the proposed OAIC were compared with those of the linear damping controller. When the fault occurred, the STATCOM with OAIC exerted a stronger damping effect on the real power than the linear damping controller (Fig. 9(a)). Moreover, in the system installed with STATCOM with the OAIC damping controller, the rotor speed and electrical torque of the wind SEIG more quickly recovered their corresponding steady states than in the system installed with the linear damping controller (Fig. 9(b) and (c)). As three-phase faults cause large fluctuations in the temporary voltage of the line bus, maintaining the transient stability of the bus voltage is normally a high priority. As shown in Fig. 9(d), STATCOM with the OAIC damping controller effectively improved the voltage transient stability, and quickly restored the voltage to its steady-state bus voltage of 1 pu.

4.4 Case 4: Performance comparison of OAIC

Panels (a), (b), and (c) of Fig. 10 compare the learning rates η_{ij}, η_{rj}, η_{jy}, η_{Ey}, and η_{ab} of FLENN and the critic network in Cases 1, 2 and 3, respectively. Because the online-tuning learning rates in the proposed OAIC are based on the GAHTVPSO algorithm, the OAIC is ideally suited to uncertain situations. Fig. 10(d) compares the convergence performances of the GAHTVPSO and three existing algorithms (modified PSO (MPSO), improved PSO (IPSO) and fuzzy PSO) (Wai et al., 2014; Yang and Kiang, 2014). The numerical results are reported in Table1. The table clarifies the higher accuracy and faster convergence rate of GAHTVPSO than the other PSO approaches. According to the convergence

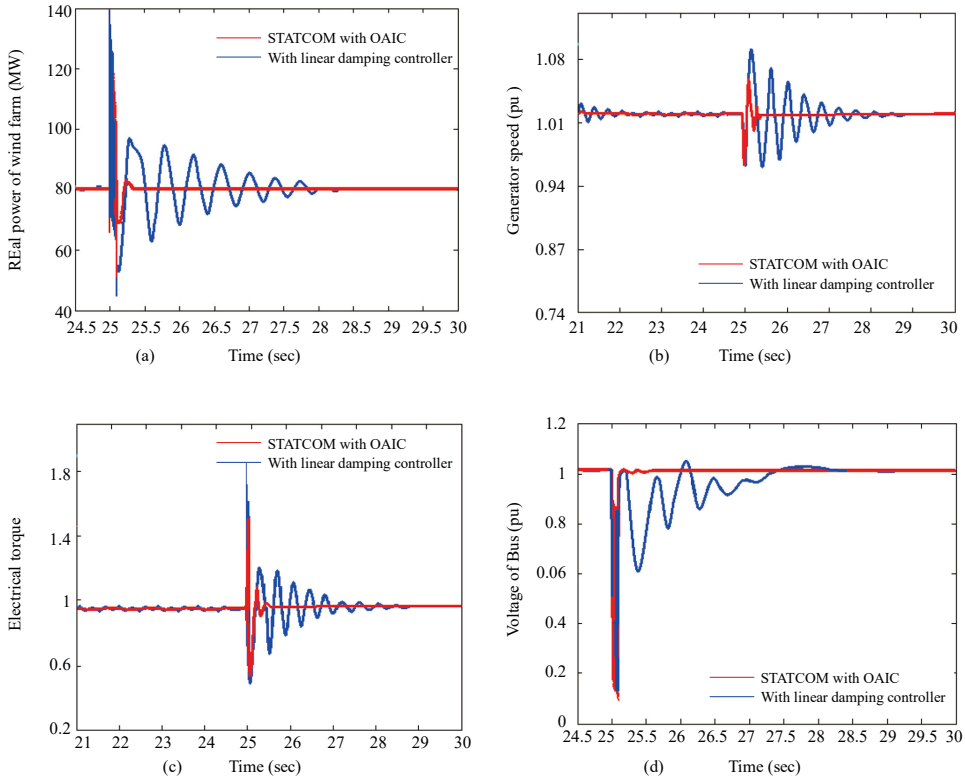

Fig. 9. Comparison results of Case 3. Plotted are (a)real power of the wind farm,(b)generator speed,(c) electrical torque responses, and (d)voltage of the bus terminal.

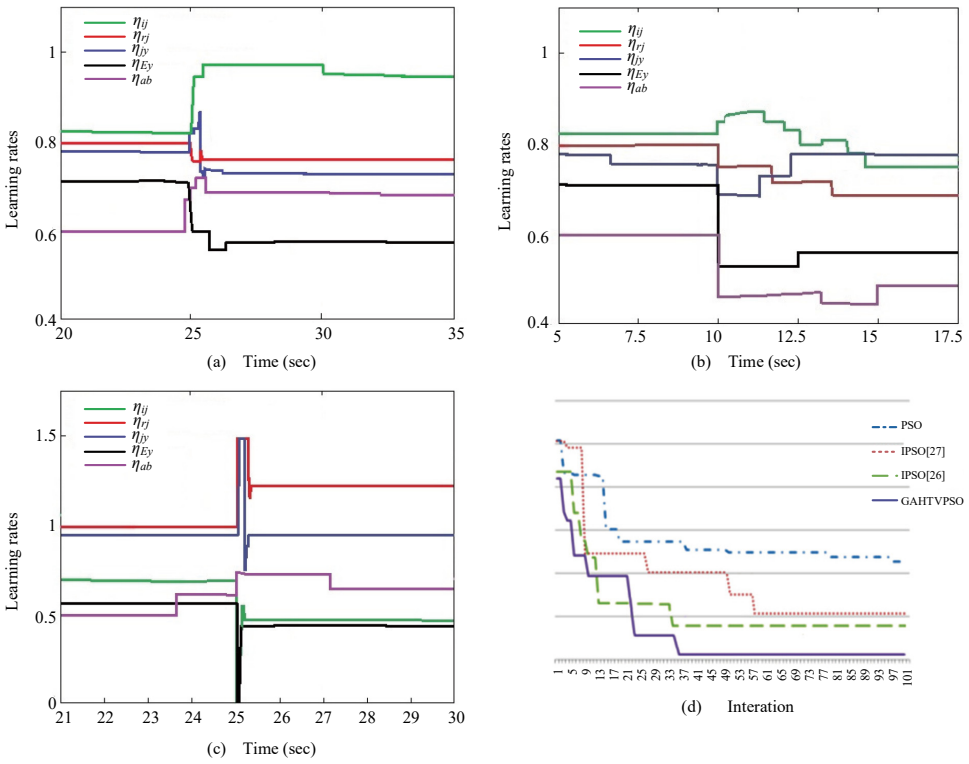

Fig. 10. Comparison results in Case 4. Panels (a), (b), and (c) plot the learning rates of FLENN and critic network in Cases 1, 2, and 3, respectively. (d) Convergence characteristics of various PSO algorithms.

characteristics of the various PSO algorithms (Fig. 10(d), the proposed algorithm better identified the nonlinear dynamic system than the other algorithms. The performance of the OAIC was further evaluated by the performance index (PI), calculated as follows (Salman et al., 2007):

$$\mathrm{PI} = \left(\sqrt{\frac{1}{N}\sum_{k=1}^{N} \Delta\omega_m^2} + \sqrt{\frac{1}{N}\sum_{k=1}^{N} \Delta V_3^2} \right) \tag{39}$$

Table2 shows the normalized results of the overall performance indices in the three case studies. The proposed OAIC damping controller for STATCOM exerted a better damping effect than the linear damping controller, reducing the oscillations in the power system by ~40%.

APPENDIX

The parameters of the system examined in this study are enumerated below.

Power system of the SEIG wind farm (Mohamed El-Moursi et al., 2010):
S=100MVA, V_S=690V, V_R=20kV, PF=0.975 lagging, X_{TS}=X_{TR}=j0.08pu, R_E=0.02498Ω, frequency=50Hz, stator resistance=0.006pu, real power=97MW, X_E=0.0899mH, X_C=4387μF, stator inductance=0.141pu, C_F=1840μF, ρ= 1.25 kg/m^3, J= 1.32×10^{-3}Nms^2, B= 5.78×10^{-3} Nm s/rad, r= 0.5m.
STATCOM with the control system (Mohamed El-Moursi et al., 2010):
$S_{STATCOM}$=70MVA, L_s=0.0001H K_{p2}=0.0015,K_{p1}=0.001, K_{i1}=0.15, K_{i2}=0, V=0.69KV, R_s=0.04Ω,frequency=50Hz
OAIC parameters:
Initial learning rates η_{ij}=η_{rj}=η_{jy}=η_{Ey}=η_{ab}=0.5, c_{1f}=c_{2f}=c_{1i}=c_{2i}=1, $c3$=1, β=0.1, α=0.1, P=15, d=5

NOMENCLATURE

ρ	air density (kg/m^3)
A	disk radius of the rotor blades (m^2)
V_ω	wind velocity (m/sec)
C_p	power coefficient
λ	tip speed ratio
ω_r	turbine speed
β	blade pitch angle
r	blade radius
T_m	mechanical torque
T_e	electrical torque
ω_e	electrical angular frequency
n_p	number of poles
J	inertia moment of WTG
B	friction coefficient of the generator
v_d	d axis stator voltages
v_q	q axis stator voltages are the
i_d	d axis stator currents
i_q	q axis stator currents
L_d	d axis stator inductance
L_q	q axis stator inductances;
λ_d	d axis stator flux linkages
λ_q	q axis stator flux linkages;
R	stator resistance;
ω_s	inverter angular frequency
I_{fd}	d-axis magnetizing current
L_{md}	d-axis mutual inductance
m	modulation index of PWM
α	phase shift of PWM
$\hat{f}_y$	outer product term
w_{Ey}	connective weight
ψ_E	function expansion output
θ	basic functions
w_{ij}	weights of the input to hidden layer
w_{rj}	weights of the context layer to hidden layer.
α	self-connecting feedback gain of context neurons
w_{jy}	weights between the hidden and multiplication layer
w_o	output layer weight
P	population size
d	particle dimensionality

REFERENCES

Chen, C. H., C. T. Lin and C. J. Lin (2007). A functional-link-based fuzzy neural network for temperature control. in Proc. IEEE Foundations of Computational Intelligence.

Chen, W. L., W. G. Liang and H. S. Gau (2010). Design of a mode decoupling STATCOM for voltage control of wind-driven induction generator systems. IEEE T Power Deliver25(3), 1758–1767.

Eberhart, R. C. and Y. Shi (2014). Fault ride-through configuration and transient management scheme for self-excited induction generator-based wind turbine. IEEE T Sustain Energ 5(1),148–159.

Elsamahy, M., S. O. Faried and T. Sidhu (2014a). Impact of midpoint STATCOM on generator loss of excitation protection. IEEE T. Power Deliver 29(2), 724–732.

Elsamahy, M., S. O. Faried and T. Sidhu (2014b). Voltage support control strategies for static synchronous compensators under unbalanced voltage sags. IEEE T Ind Electron 61(2), 808–820.

Fan, L. and Z. Miao (2012). Mitigating SSR using DFIG-based wind generation. IEEE T Sustain Energ 3(3), 349–358.

Farkhani, J. S. and H. R. Najafi (2014). Sensitivity analysis of nonlinear dynamic behavior of self excited induction generator (SEIG) in wind turbine. International Journal on "Technical and Physical Problems of Engineering 18(6), 101–107.

Farrag, M. E. A. and G. A. Putrus (2012). Design of an adaptive neuro fuzzy inference control system for the unified power-flow controller. IEEE T Power Deliver.27(1), 53–61.

George, N. V. and G. Panda (2012). A particle-swarm-optimization-based decentralized nonlinear active noise control system. IEEE T Instru Meas 61(12), 3378–3386.

Golshannavaz, S., M. Mokhtari and D. Nazarpour (2011). SSR suppression via STATCOM in series compensated wind farm integrations. Proc. 19th. ICEE1–6.

Hong, Y. Y. and Y. F. Luo (2009). Optimal VAR control considering wind

farms using probabilistic load-flow and gray-based genetic algorithms. IEEE T Power Deliver 24(3), 1441–1449.

Li, W. and T. Dinh-Nhon (2013). Stability enhancement of DFIG-based offshore wind farm fed to a multi-machine system using a STATCOM. IEEE T Power Syst 28(3), 2882–2889.

Lin, F. J., L. T. Teng, J. W. Lin and S. Y. Chen (2009). Recurrent functional link based fuzzy neural network controlled induction-generator system using improved particle swarm optimization. IEEE T Ind Electron56(5), 1557–1577.

Lin, W. M., C. M. Hong, C. H. Huang and T. C. Ou (2013). Hybrid control of a wind induction generator based on Grey–Elman neural network. IEEE T Control Systems Tech 21(6), 2367–2373.

Lin, W. M., C. M. Hong, T. C. Ou and T. M. Chiu (2011). Hybrid intelligent control of PMSG wind generation system using pitch angle control with RBFN. Energ Convers Manage 52(2), 1244–1251.

Lin, W. M., K. H. Lu, C. H. Huang, T. C. Ou and Y. H. Li (2009). Optimal location and capacity of STATCOM for voltage stability enhancement using ACO plus GA. Proc IEEE/ASME, 1915–1920.

Mohamed El-Moursi, S., B. Bak-Jensen and H. Abdel-Rahman (2010). Novel STATCOM controller for mitigating SSR and damping power system oscillations in a series compensated wind park. IEEE T Power Electr 25(2), 429–441.

Salman, M., G. K. Venayagamoorthy and R. G. Harley (2007). Optimal neuro-fuzzy external controller for a STATCOM in the 12-bus benchmark power system. IEEE T Power Deliver 22(4), 2548–2558.

Singh, B., S. S. Murthy and R. S. R. Chilipi (2014). STATCOM-based controller for a three-phase SEIG feeding single-phase loads. IEEE T Energy Conver29(2), 320–331.

Srivastava, L., S. Dixit and G. Agnihotri (2012). Position mutated hierarchical particle swarm optimization and its application in synthesis of unequally spaced antenna arrays. IEEE T Antenn Propag 60(7), 3174–3181.

Srivastava, L., S. Dixit and G. Agnihotri (2014). Optimal location and size of TCSC for voltage stability enhancement using PSO-TVAC. Proc PESTSE, 1–6.

Swakshar, R. and K. V. Ganesh (2008). Wide-area signal-based optimal neurocontroller for a UPFC. IEEE T Power Deliver 2(3), 1597–1605.

Swakshar, R. and K. V. Ganesh (2013). Online learning control using adaptive critic designs with sparse kernel machines. IEEE T Neur NetLear 24(5), 762–775.

Toh, K. A. and W. Y. Yau (2005). Fingerprint and speaker verification decisions fusion using a functional link network. IEEE T Syst Man Cy C35(3), 357–370.

Wai, R. J., S. Cheng, Y. F. Lin and Y. C. Chen (2014). Installed capacity selection of hybrid energy generation system via improved particle-swarm-optimisation IET. Gener Transm Dis 8(4), 742–752.

Waldner, M. and I. Erlich (2014). Variable speed wind turbines based on electromechanical differential systems. IEEE T Energy Conver29 (1), 101–109.

Yang, S. H. and J. F. Kiang (2014). Optimization of asymmetrical difference pattern with memetic algorithm IEEE T Antenn Propag 62(4), 2297–2302.